MULTIPLE APERTURE INSAR (MAI) WITH C-BAND AND L-BAND DATA: NOISE AND PRECISION

Noa Bechor Ben-Dov and Thomas A. Herring

Massachusetts Institute of Technology, Cambridge, MA 02139, USA, Email: nbechor@chandler.mit.edu

ABSTRACT

MAI is a technique to extract along-track (horizontal) phase-based displacements from InSAR data. MAI's theoretical precision can be at the centimeter level, an order of magnitude improvement over amplitude-based pixel offset approaches. However, MAI has been challenging to implement with most academic InSAR processors, and the theoretical precision difficult to reach for low to medium coherence terrains. We implement MAI with the JPL/CALTECH InSAR processor ROI_PAC. We study the MAI noise structure with Envisat, Radarsat-1, ERS, and ALOS data, and develop phase corrections and filtering based on the results.

We study the MAI noise with 'zero' signal, all noise data. We process 11 Envisat pairs presenting low to medium coherence with less than 2 cm along track displacements, taken over the larger Los Angeles basin/San Gabriel Mountains in California, US. The test data contain a variety of decorrelation sources and cover different types of terrain, including urban, mountainous, vegetated and sea surfaces, as well as variety in temporal and spatial baselines. To test the MAI filter we superimpose the MAI noise images with signal simulating coseismic displacements from the 1812 Mw 7 Wrightwood earthquake sequence. The results present a correlation dependent RMSE ranging from 8 cm in correlation coefficient 0.4 to 2 cm in correlation coefficient 0.75. In an actual signal case (Hawaii, L-band), the random component of the noise for correlation coefficient of 0.5 to 0.95 varies from 2 cm to 4 mm.

Key words: InSAR; MAI; Along-track interferometry.

1. INTRODUCTION

Space-based InSAR has an essential flaw built into most systems: with the exception of polar regions, it can provide at best up to 2-D measurements. The third dimension information is oriented in the satellite's along-track direction. Two techniques are available to extract along-track information from repeat SAR data: amplitude based sub-pixel offsets (Michel et al. 1999) and phase based

Multiple Aperture InSAR, or MAI, (Bechor & Zebker 2006; Bechor 2007). MAI is a technique to generate along-track phase measurements by splitting the beam to forward- and backward-looking parts. Studies comparing MAI phase measurements to amplitude sub-pixel offsets find approximately a factor of 2 improvement in noise levels (Bechor & Zebker 2006; Barbot et al. 2008; Gourmelen et al. 2011). While MAI found use in several studies (Barbot et al. 2008; Lu & Dzurisin 2010; Biggs et al. 2009; Jung et al. 2011; Gourmelen et al. 2011), its use remained restricted to large signals and/or very high coherence terrains. This is largely due to the MAI phase noise, which contains large amounts of speckle noise in addition to reduced levels of other InSAR noise sources (Bechor & Zebker 2006; Jung et al. 2009).

Three MAI implementations were proposed: Bechor & Zebker (2006) split the beam by restricting the azimuth resolution and focusing the forward-/backward-looking scenes to a squinted Doppler centroid. Barbot et al. (2008) bandpass filter the already focused SLC's to seperate the scene into forward- and backward- looking parts, and Jung et al. (2009) employ a similar approach to Bechor & Zebker (2006), though with a skewed geometry. They encounter and resolve shifts between the subapertures, and need to focus the forward-/backward-looking scenes with a common range migration correction. While all three studies were done on high coherence terrain (desert), their reported precision differs. Bechor & Zebker (2006) report a coherence-dependent precision. They compare their results to GPS observations and find precision from 5 cm to 8.8 cm. Barbot et al. (2008) suggest a 10 cm precision on their implementation, and Jung et al. (2009) find gradients in order of over 2 meters across the scene, and report a standard deviation of 10.2 to 13.1 cm following their correction.

Here we study the MAI noise. We focus our attention on low to medium coherence terrains, and study both spatially correlated noise in the form of gradients and random noise (mostly in the form of speckle) using 11 Envisat ASAR interferometric pairs. We implement the (Bechor & Zebker 2006) approach with the JPL/CALTECH processor ROI_PAC (Massonnet & Feigl 1998; Thompson et al. 1986; Rosen et al. 2000; Zebker & Goldstein 1986; Rosen et al. 2004), and find phase gradients of up to 15 cm across the scene. We find that for correlation coefficient levels above 0.4 filtering a single
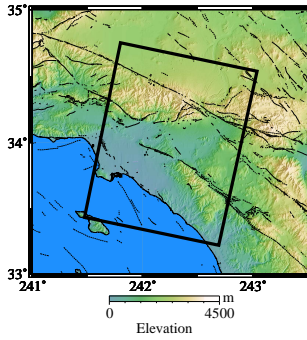
Figure 1. Test site location map. The dark rectangle illustrates the Envisat strip-mode data location. We use 11 interferograms taken from 2004/08/06 to 2005/12/10, with temporal baselines from 1 to 6 months. Data by ESA, made available to us through the WInSAR consortium.

interferometric pair reduces the random noise to between 8 cm to 4 millimeters, depending on terrain type.

2. DATA

We use one data set to test the processor and study the MAI noise distribution, and an independent data set to evaluate its performance under different conditions.

The test data contains 12 Envisat scenes collected over the larger Los Angeles Basin/San Gabriel Mountains in California, USA (Figure 1). We process them into 11 interferometric pairs with temporal baselines that vary from one month to one year.

The test area contains a vriety of terrains: mountains, urban areas, sea, forest, and desert with some vegetation, allowing us to study the MAI noise distribution with these decorrelation sources. In addition, the test area is densely covered with a continous GPS network. King et al. (2007) use the GPS data to study the displacement field during 2005. The along-track projection of the GPS displacements is less then 1 cm, below any precision that has (so far) been achieved with MAI (Bechor & Zebker 2006; Jung et al. 2011; Gourmelen et al. 2011). The 11 test pairs therefore represent repeated measurements of the MAI noise - related to both decorrelation and any other noise sources, such as atmospheric, orbital, and those related to Earth's shape.

We process additional data in order to evaluate the processor's performance with independent data sets. We choose an ALOS PALSAR interferogram spanning the Hawaii Father's Day intrusion.

3. MAI PROCESSOR AND FILTER

MAI data processing involves splitting the Doppler spectrum into two parts to form forward- and backward-

oriented SLCs, and forming the respective forward- and backward-looking interferograms. Their phase difference largely represents phase change due to along-track displacements. We implement the (Bechor & Zebker 2006) implementation for the JPL/CALTECH InSAR processor ROI_PAC (Massonnet & Feigl 1998; Thompson et al. 1986; Rosen et al. 2000; Zebker & Goldstein 1986; Rosen et al. 2004). This largely required adding (more precisely, maintaining) a 'deskew' option to the SAR processor.

MAI phases contain high levels of speckle noise. This means that filters which were designed for lower speckle distributions, such as InSAR interferograms, may not provide optimal results. We therefore filter the data with a phase preserving filter which we designed specifically for high speckle MAI phase maps.

4. EXPERIMENT DESIGN

We evaluate both the MAI precision and the filter's performance for the test case. We first process the data using the renewed JPL/CALTECH ROI_PAC processor. The results form our empirical MAI noise interferograms (Figure 2c). To these we add simulated signal from the slip distribution of the 1812 Wrightwod earthquake(Jacoby et al. (1988); Deng & Sykes (1997); Toppozada (2002), Figure 2b). We produce the simulated displacements with Green's functions in elastic half space (OKADA 1992), and project them to the along-track direction. We then translate them to phase and supersimpose them on the empirical MAI noise maps. The resulting known-signal, known-noise MAI phases (translated back to displacements in Figure 2d) form the input data for the filter evaluation.

We also filter the noise-only interferograms. This serves three purposes: (1)evaluate the level of spatially correlated noise in the form of phase gradients; (2) allow for quantifying the random component of the MAI noise separately from the spatially correlated signals; (3) evaluate the filter for biases: an unbiased filter would produce results that, once corrected for the signal, are identical to the filtered noise interferograms. We contrast the two results both qualitatively and quantitatively.

Once the filter is verified, we check if the filter is useful also for an independent high coherence cases. We process and filter MAI data from Hawaii's Father's Day intrusion, spanning May to June 2007, and evaluate random noise levels in the results.

5. RESULTS

5.1. Processor and Filter Evaluation: General Features

Phase gradients in the results reach up to 1.5 millimeter/kilometer (Figure 2f). These are at times accompa-
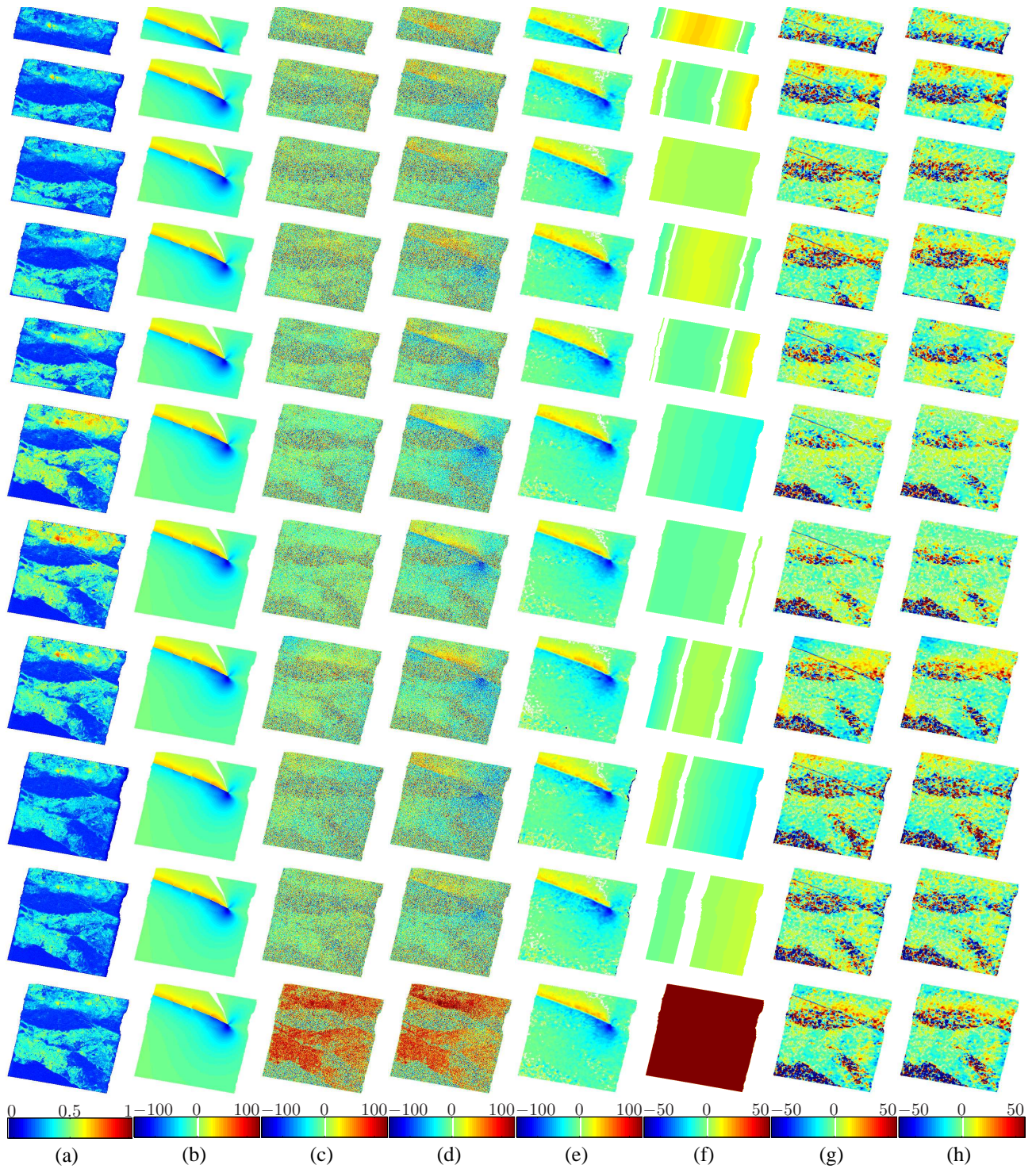
Figure 2. Filtering results. (a) InSAR correlation coefficient ('coherence') (b) simulated signal in centimeters (c) MAI noise interferograms from the greater LA area (d) superposition of signal and noise; (e) IHF filtering results; (f) gradients; (g) residuals; (h) filtered noise interferograms. All scales are in centimeters unless otherwise noted.

nied by a constant, of up to ZZ cm (pair 11 on Figure 2f). These gradients are the highest in virtually in all the data sets that we happened to test. We suspect that the gradients are larger because of orbital errors in the input parameters to the SAR processor, as we cut the data from long strip-mode Envisat scenes. Whatever the cause may be, gradient levels of 1.5 millimeter/km are lower then the 20 millimeter/km levels reported elsewhere (Jung et al. 2009).

Figures 2d and 2e contain the pre- and post-filtering results, respectively. The pre-filtering (input) data exhibit high speckle, though signal in the levels of ± 30 centimeters is visually detectable. In the post-filtering results low-correlation areas exhibit random behavior (i.e. contrast Figure 2d with the correlation coefficient maps on Figure 2a), and signal is visually detectible to a level of zero to 1 centimeters in many of the images (i.e. most prominently in pairs 4, 5, 6, 7 on Xe).

We calculate residuals by removing the simulated signal (Figure 2c) from the filtering results (Figure 2e). With the exception of the fault trace, the resulting residuals (Figure 2g) are visually identical to the filtered MAI noise interferograms in Figure 2h. With the fault trace masked, the root residual sum of squares (RRSS) of the difference between the two is MM cm, suggesting the filter is unbiased with respect to signal level. Figure 3 displays the RRSS of the residuals (diamonds) and noise interferograms (line). The agreement between the two again suggests the filter is unbiased.

We note the existence of spatially correlated noise in the MAI images. This noise ranges from ± 5 centimeters on the pairs with shortest temporal baselines (pairs 6,7 in Figure 2h) to a maximum of ± 20 centimeter in some of the other pairs (pairs 2, 7). The spatially correlated noise varies with time and space, which may suggest an atmospheric origin.

5.2. MAI's Precision in Low to Medium Correlation Levels

We use the residuals (Figure 2g) to estimate the MAI precision with coherence. Figure 3 shows the root mean square error (RMSE) with correlation coefficient for all the pixels in the experiment in black, and RMSE for specific terrains in blue. The black line represents the RMSE for the noise interferograms in Figure 2h; diamonds denote the RMSE for the residuals in Figure 2g. We calculate the RMSE as the root residual sum of squares (RRSS), which is a measure of RMSE in sufficiently large sample sizes. With the exception of gradients, the results in Figure 3 contain any spatially correlated noise that is present in the data.

As expected, precision increases with coherence. Starting from the lowest correlation coefficient, the RRSS decreases quickly as the correlation coefficient (γ) rises, until approximately $\gamma = 0.4$, where the RRSS is ~ 0.8 centimeters. Above $\gamma = 0.4$ the precision improves more
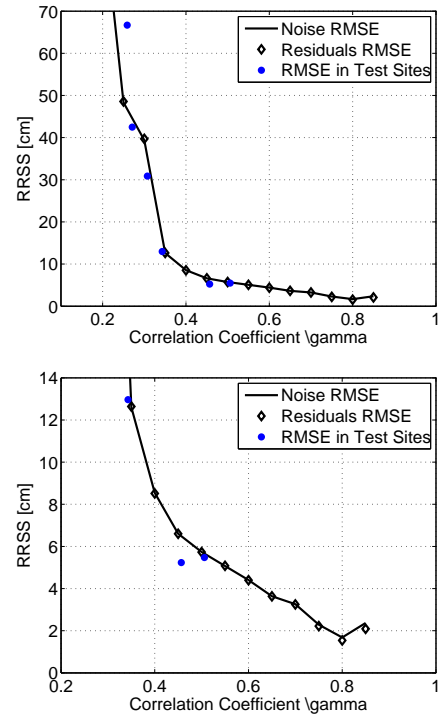

Figure 3. Root residual sum of squares (RRSS, a measure of RMSE) calculated for pixels sorted by coherence bins. Top: full scope. Bottom: zoom on useful range. Solid line: noise interferograms. Diamonds: Residuals from simulated signal + actual noise experiment. Blue dots: results in smaller regions with specific terrain types.

slowly, reaching 2 centimeters at $\gamma = 0.75$ and above. Pixels for these high correlation levels come primarily from the two pairs with 1 month temporal baseline (pairs 6,7), and are fewer in numbers then the low to medium coherence level pixels.

The RMSE for specific terrains also behaves as expected. We find 6 areas with distinct terrain types. From high to low RMSE: sea (66 cm), forested mountains (42 cm), sparsly forested mountains (30 cm), mountains with a mix of urban and forest cover (12 cm), partially decorrelated desert (5.5 cm), and flat urban (5.0 cm). The surprising find is that the RMSE of specific terrains behaves similarly to the RMSE of all the pixels with the same correlation coefficient. The one exception is in the flat urban terrain, which presents a 5 cm error instead of a 6 cm error for its correlation level. This could be due to the many point-like scatteres in man-made enviroments.

5.3. MAI Noise in an Independent High Coherence Case

We process and filter ALOS PALSAR data (L-band) from the Hawaii Father's Day intrusion to evaluate the processor and filter in an independent case with high coherence. Figure 4 displays the InSAR correlation coefficient and
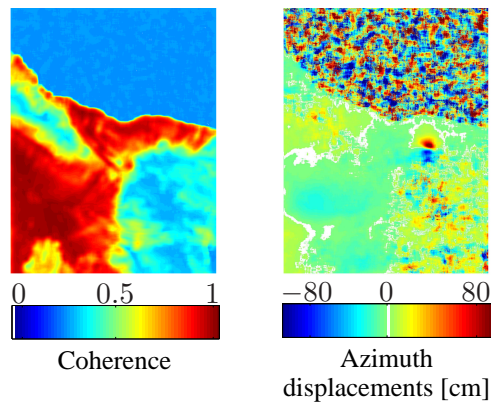
Figure 4. High Coherence Case. Right: correlation coefficient. Left: MAI displacements.

the MAI displacements. Both figures are in radar coordinates: the sea is the uncorrelated section in the upper part of the figures, and the intrusion is in the middle and to the right. We note the expected behavior of random noise with coherence, as well as the existence of spatially correlated signatures in the order of ± 15 centimeters.

We next evaluate the level of random noise. We fit a surface to the signal, remove it, and calculate the RRSS of the residuals. We expect the experiment to show better precision levels then in Figure 4, as when fitting the surface we likely remove most of the spatially correlated noise, while in the previous experiment these noise sources where part of the precision calculation. The resulting RRSS for $\gamma = 0.5$ is 2 centimeters. For the highest values of correlation coefficient ($\gamma = 0.9$ to 1) the RRSS is down to 4 millimeters.

6. CONCLUSIONS

We implement MAI data processing with the JPL/CALTECH InSAR processor ROI_PAC. We use the implementation by Bechor & Zebker (2006), and filter the processed MAI images with a phase preserving filter designed specifically for high speckle phase noise. We test the processor and filter performance with 11 Envisat ASAR interferometric pairs and one ALOS PALSAR pair. Together, the two data sets contain N pixels with associated correlation coefficient of low (0-0.4), medium (0.4-0.75) and high (0.75-1) values. Our finding are:

- Gradients in the across track direction of up to 1.5 millimeter/km.

- None-gradient, arbitrarily oriented spatially correlated noise of up to ± 15 centimeters, variable in time and space.

- Coherence-dependent noise. Taken together, for correlation coefficient $\gamma = 0.4$ and above, the random and variable spatially correlated noise compo-

nents result in precision that varies from 8 to 2 centimters in C-band.

- In $\gamma = 0.5$ and above, the random noise alone varies from 2 centimeters to 4 millimeters in L-band.

REFERENCES

Barbot, S., Hamiel, Y., & Fialko, Y. 2008, J. Geophys. Res, 113, B03403

Bechor, N. 2007, PhD thesis, Stanford University

Bechor, N. & Zebker, H. 2006, Geophysical Research Letters, 33, 16311

Biggs, J., Amelung, F., Gourmelen, N., Dixon, T. H., & Kim, S.-W. 2009, Geophysical Journal International, 179, 549

Deng, J. & Sykes, L. R. 1997, Journal of Geophysical Research, 102, 9859

Gourmelen, N., Kim, S. W., Shepherd, A., et al. 2011, Earth and Planetary Science Letters, 307, 156

Jacoby, G. C., Sheppard, P. R., & Sieh, K. E. 1988, Science, 241, 196

Jung, H., Won, J., & Kim, S. 2009, IEEE Transactions on Geoscience and Remote Sensing, 47, 2859

Jung, H. S., Lu, Z., Won, J. S., Poland, M. P., & Miklius, A. 2011, IEEE Geoscience and Remote Sensing Letters, 8, 34

King, N. E., Argus, D., Langbein, J., et al. 2007, Journal of Geophysical Research (Solid Earth), 112, B03409

Lu, Z. & Dzurisin, D. 2010, Journal of Geophysical Research (Solid Earth), 115, B00B03

Massonnet, D. & Feigl, K. 1998, Rev. Geophys, 36, 441

Michel, R., Avouac, J.-P., & Taboury, J. 1999, Geophysical Research Letters, 26, 875

OKADA, Y. 1992, BULLETIN OF THE SEISMOLOGICAL SOCIETY OF AMERICA, 82, 1018

Rosen, P., Hensley, S., Joughin, I., et al. 2000, Proceedings of the IEEE, 88, 333

Rosen, P., Hensley, S., Peltzer, G., & Simons, M. 2004, Eos Trans. AGU, 85, 47

Thompson, A. R., Moran, J. M., & Swenson, G. W. 1986, Interferometry and synthesis in radio astronomy (New York, Wiley-Interscience, 1986, 554 p.)

Toppozada, T. R. 2002, The Bulletin of the Seismological Society of America, 92, 2555

Zebker, H. & Goldstein, R. 1986, Journal of Geophysical Research, 91